Supporting Information

Content

Fig. S1. ^{1}H NMR spectrum of **1** in $CDCl_3$ at 27 °C.	2
Fig. S2. ^{13}C NMR spectrum of **1** in $CDCl_3$ at 27 °C.	3
Fig. S3. ^{1}H NMR spectrum of **2** in $CDCl_3$ at 27 °C.	4
Fig. S4. ^{13}C NMR spectrum of **2** in $CDCl_3$ at 27 °C.	5
Fig. S5. FT-IR spectra of IPr*Se, **1**, and **2** (Neat).	6
Fig. S6. ^{1}H NMR spectrum of **3** in DMSO-d_6 at 27 °C.	7
Fig. S7. ^{13}C NMR spectrum of **3** in DMSO- d_6 at 27 °C.	8
Fig. S8. Neat FT-IR spectrum of **3**.	9
Fig. S9. ^{1}H NMR spectrum of **4** in DMSO-d_6 at 27 °C.	10
Fig. S10. ^{13}C NMR spectrum of **4** in DMSO-d_6 at 27 °C.	11
Fig. S11. Neat FT-IR spectrum of **4**.	11
Fig. S12 Top: TGA profiles of IPr*Se, **1**, and **2** from 35 °C to 700 °C recorded with a heating rate of 10 °C min^{-1} under the nitrogen atmosphere. Bottom: TGA curves of [(IPaul)Se], **3**, and **4** from 35 °C to 800 °C recorded with a heating rate of 10 °C min^{-1} under the nitrogen atmosphere	12
Table S1. Crystal data and structure refinement parameters for **1, 2**, **3,** and **4**.	13
Fig. S13. Optimized geometry of **1A** at the B3LYP/Def2TZVP, 6-31++G** level.	14
Fig. S14. Optimized geometry of **1B** at the B3LYP/Def2TZVP, 6-31++G** level.	15
Fig. S15. Comparison of HOMO-LUMO energy gap in **1A** and **1B**.	16
Fig. S16. Lone pairs (HOMO-6) on antimony in **1A.**	17
Fig. S17. Lone pair of electrons in **1A.**	17
Fig S18. AIM analysis of **1A.**	18
Table S2. The Cartesian coordinates of **1A** optimized at the B3LYP/Def2TZVP,6-31++G** level.	19
Table S3. Donor-Acceptor interaction in complex **1A.**	21
Table S4. Orbital occupancy, hybridization of orbitals involved in donor-acceptor interaction in **1A.**	22
Table S5. Topological properties of the electron density computed at BCP's for **1A** computed at the B3LYP level.	23
Table S6. Orbital occupancy – Valence orbitals of **1A**.	24
Table S7. Natural Population Analysis of **1A**.	24
Table S8. Electronic configuration of selected atoms of **1A**.	25
Table S9. Wiberg Bond Index of **1A**.	25
Table S10. The Cartesian coordinates of **1C** optimized at the B3LYP/Def2TZVP, 6-31++G** level.	26
Table S11. The Cartesian coordinates of **1D** optimized at the B3LYP/Def2TZVP, 6-31++G** level.	28
Crystallographic analysis of **1-4**	30-32
References	33

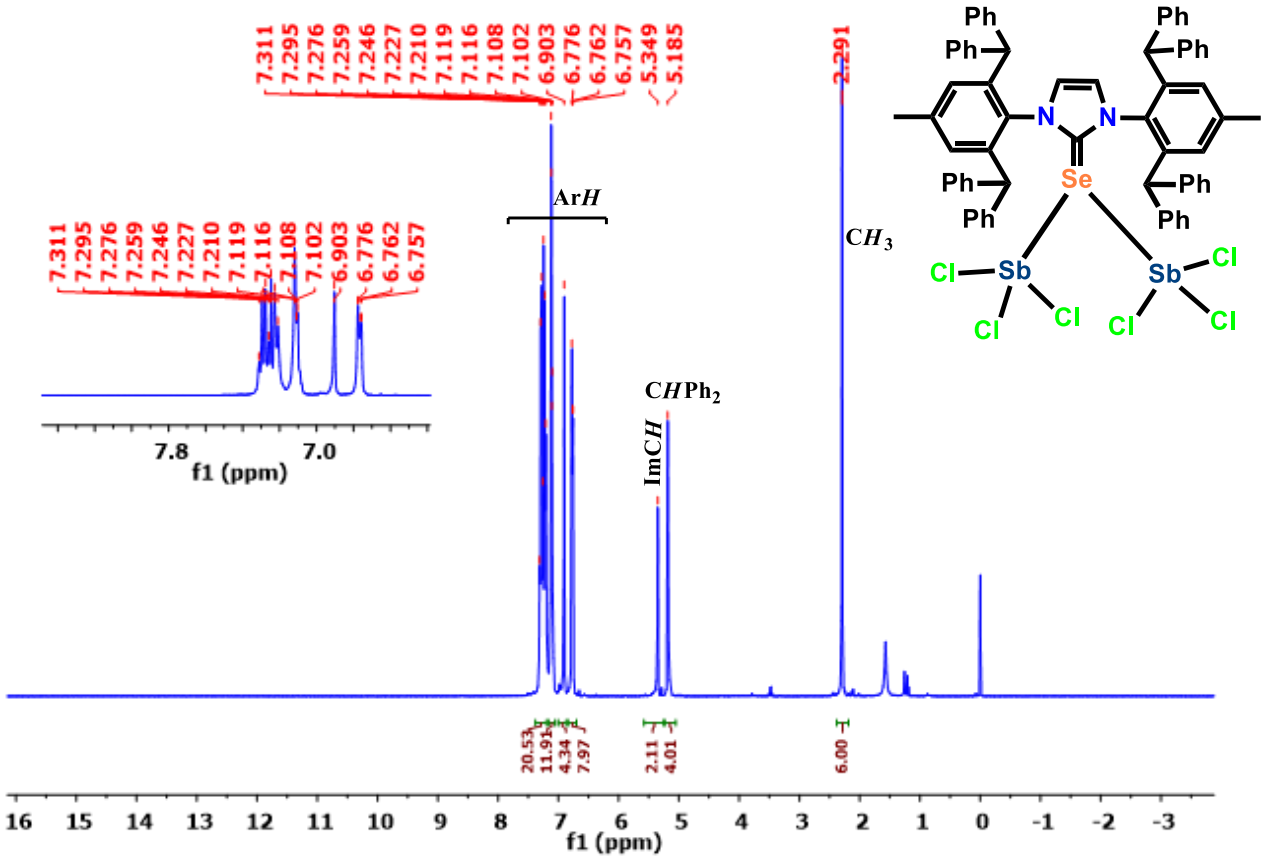

Fig. S1. ^{1}H NMR spectrum of **1** in $CDCl_3$ at 27 °C.

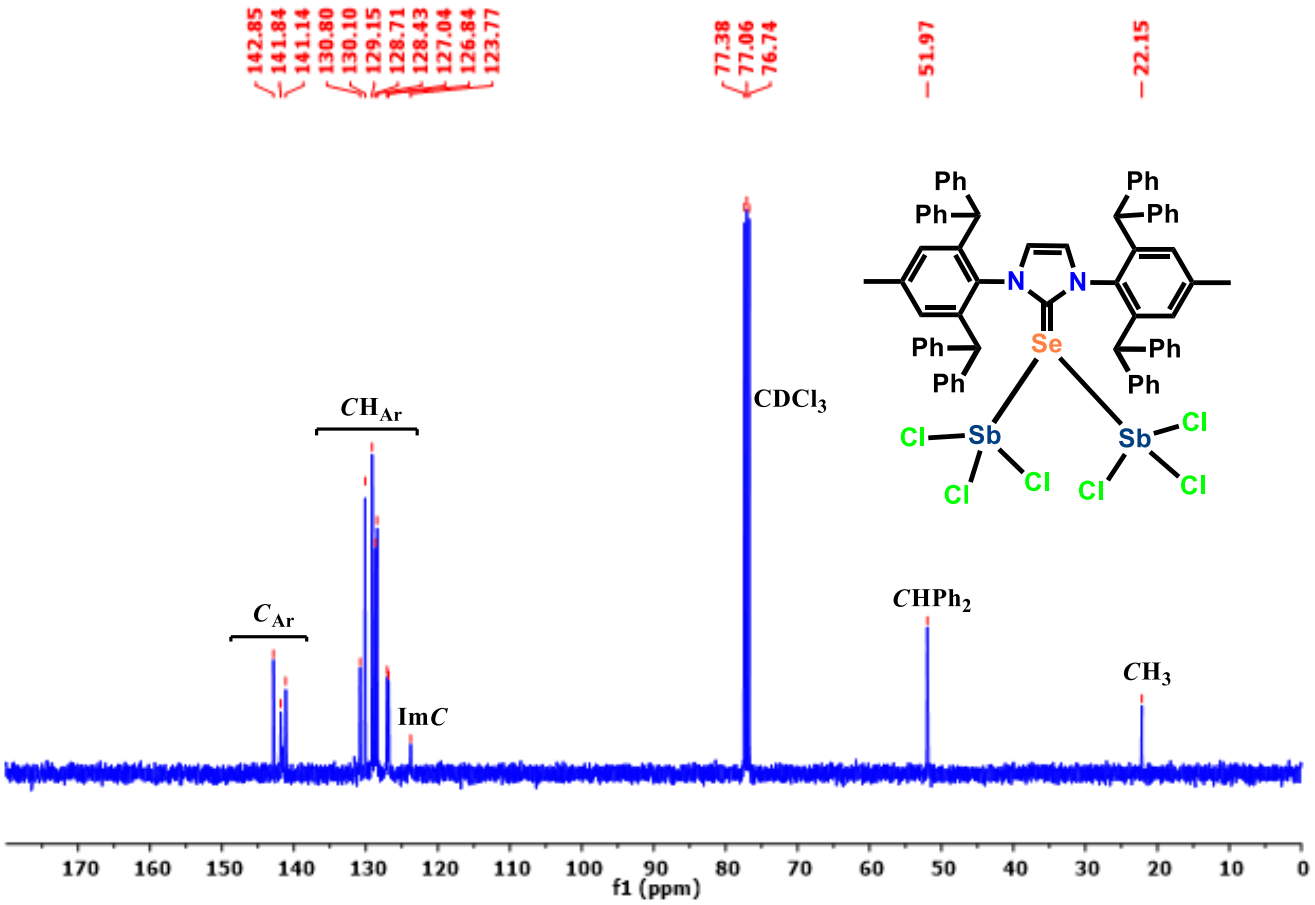

Fig. S2. ^{13}C NMR spectrum of **1** in $CDCl_3$ at 27 °C.

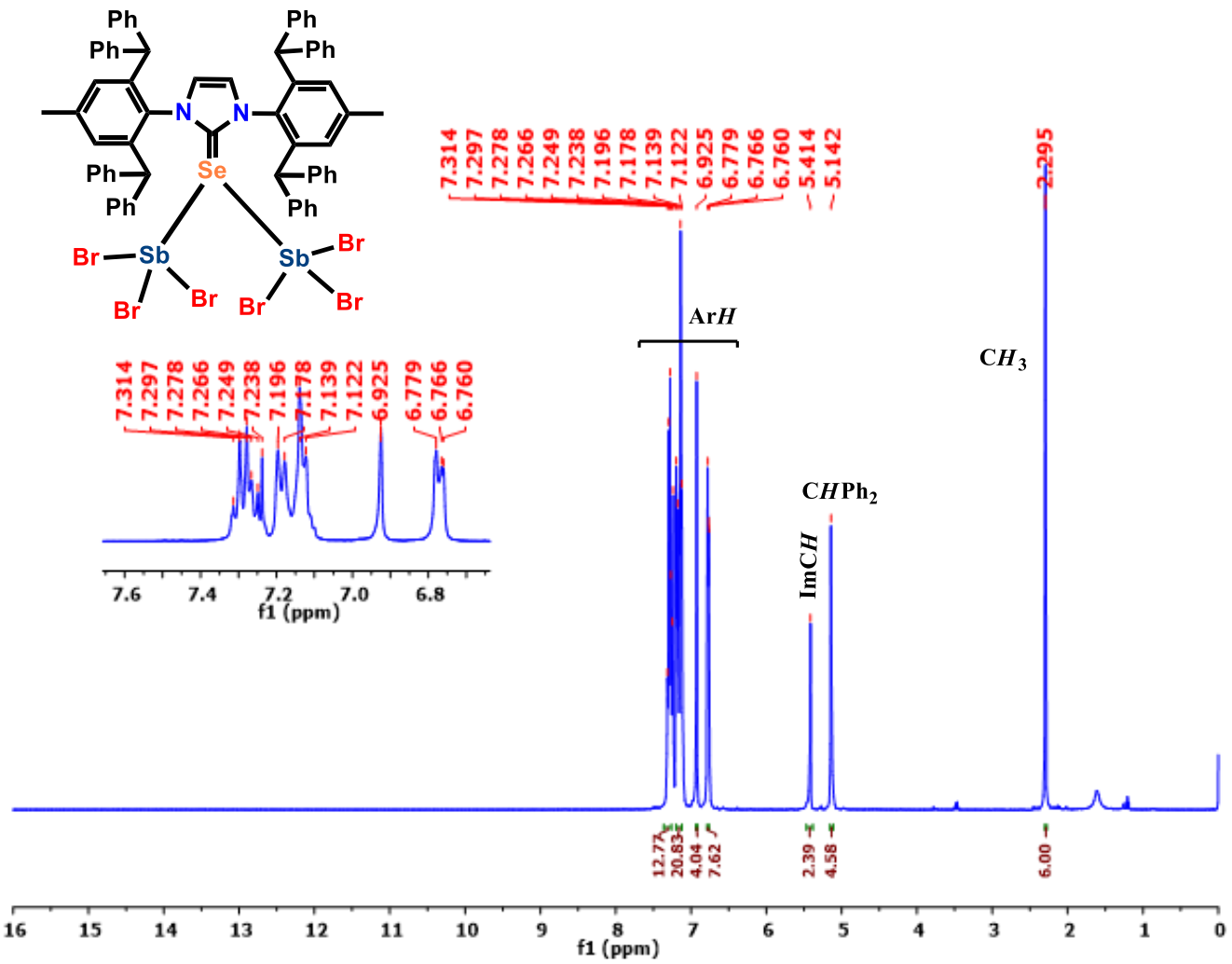

Fig. S3. ^{1}H NMR spectrum of **2** in $CDCl_3$ at 27 °C.

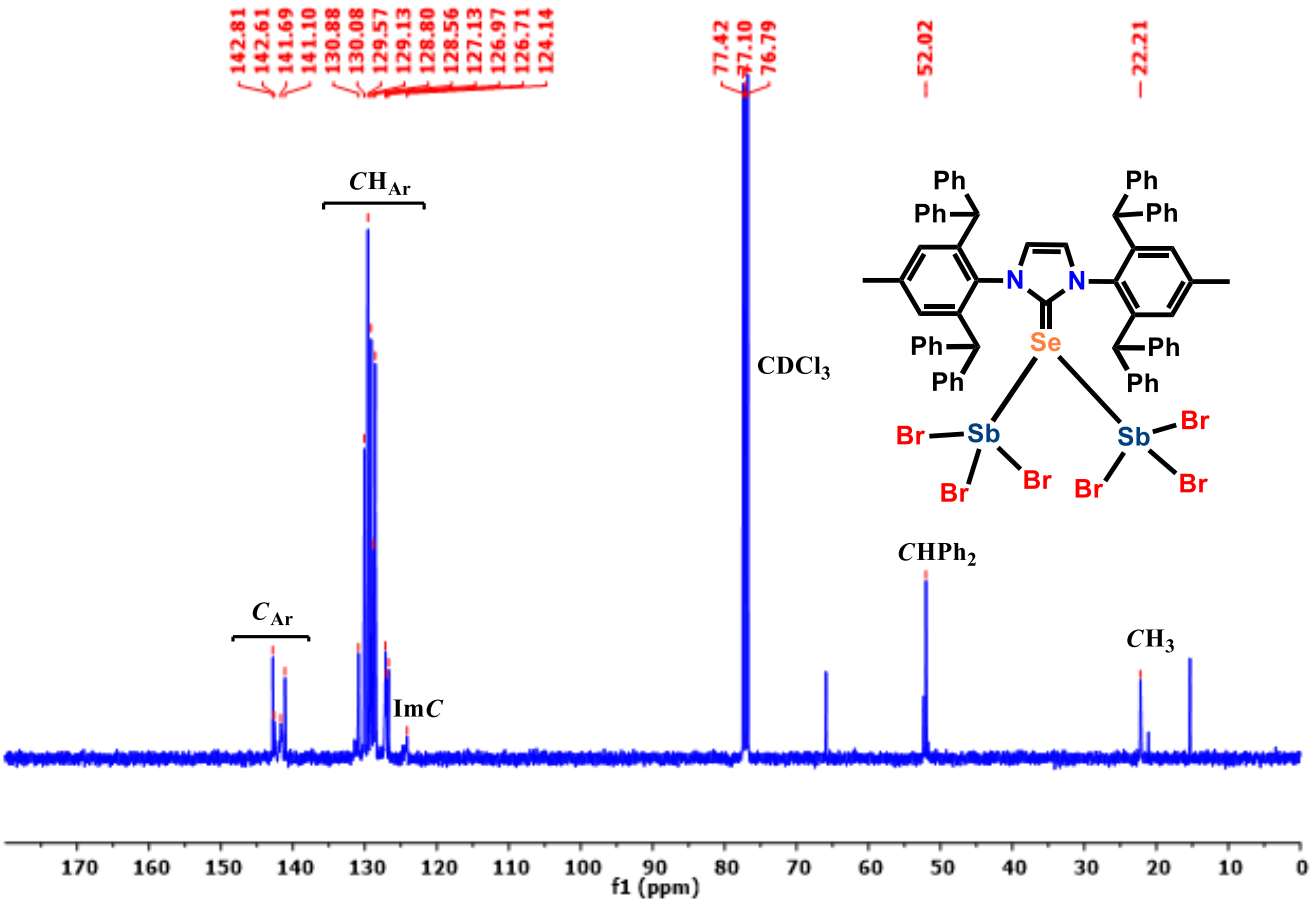

Fig. S4. ^{13}C NMR spectrum of **2** in $CDCl_3$ at 27 °C.

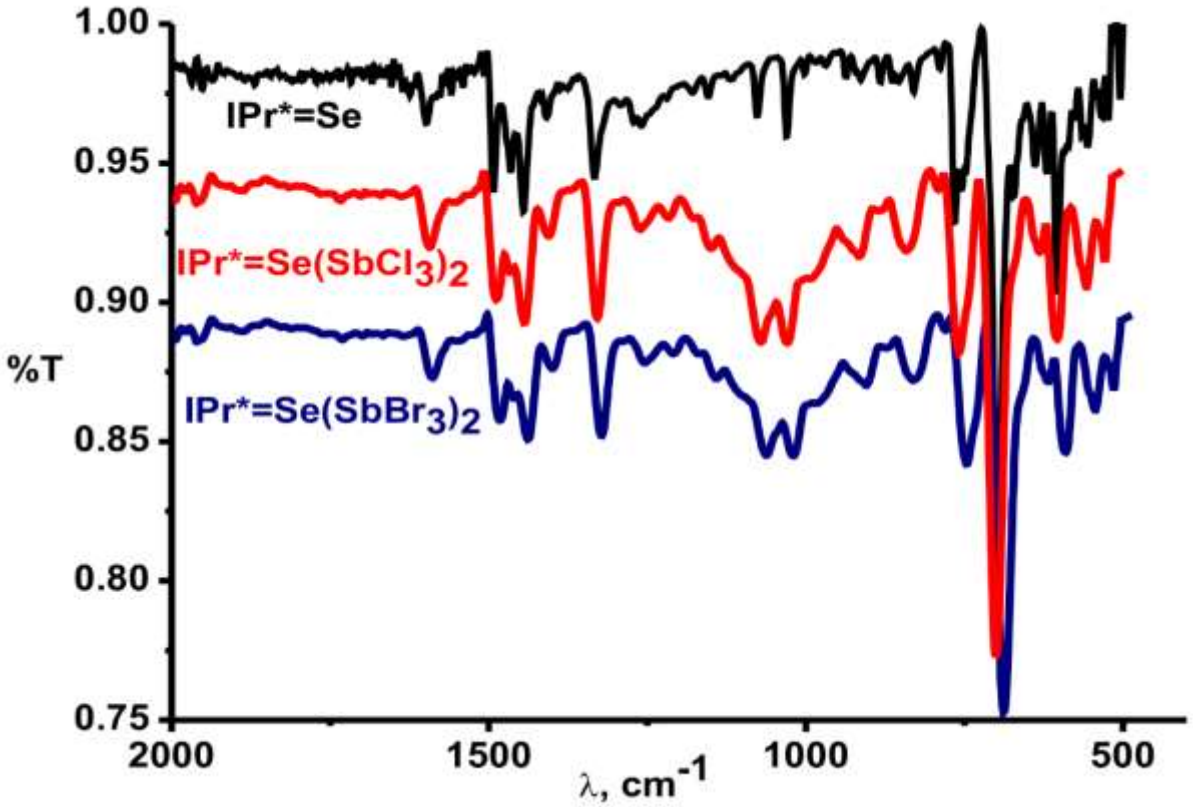

Fig S5. FT-IR spectra of IPr*Se, **1**, and **2** (Neat).

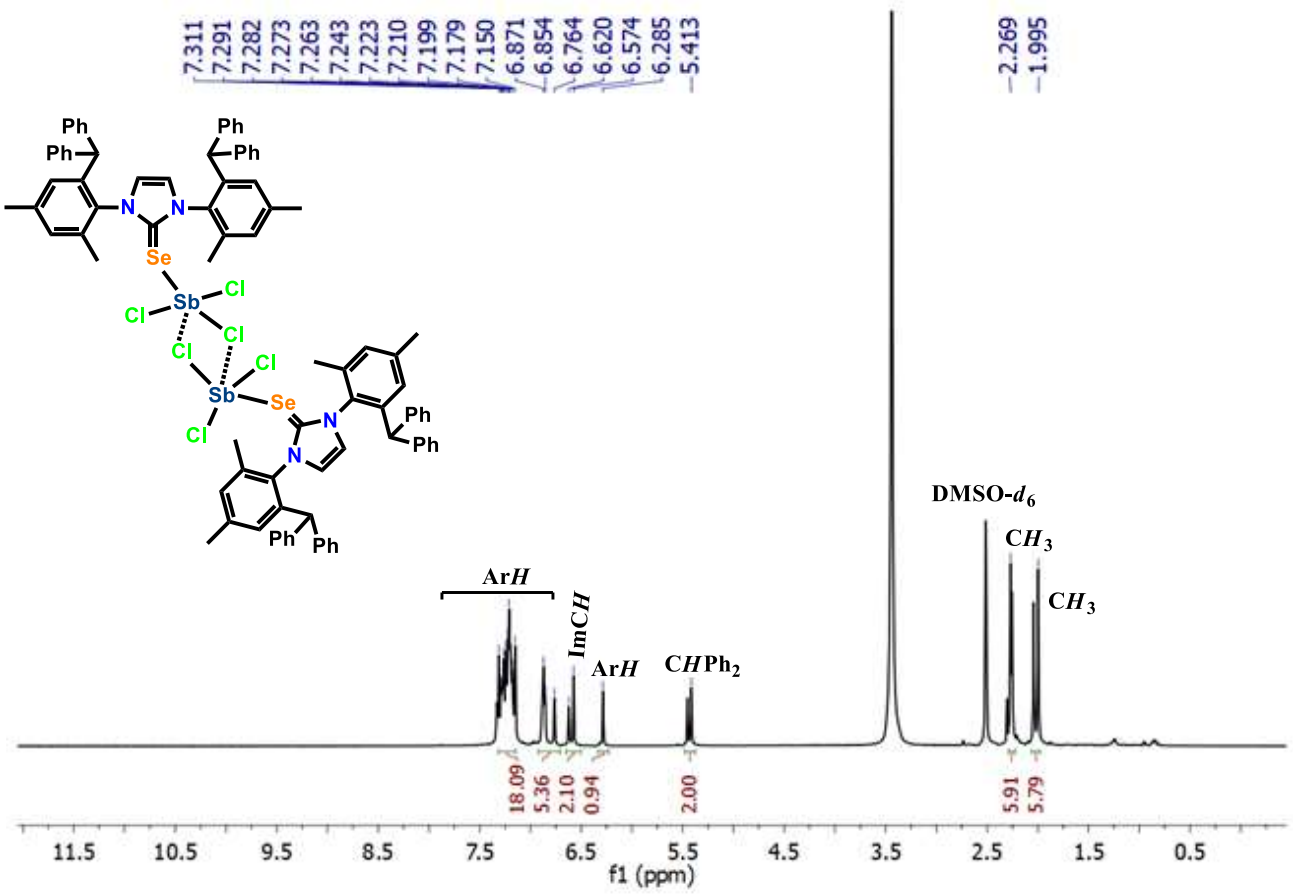

Fig. S6. ^{1}H NMR spectrum of **3** in DMSO-d_6 at 27 °C.

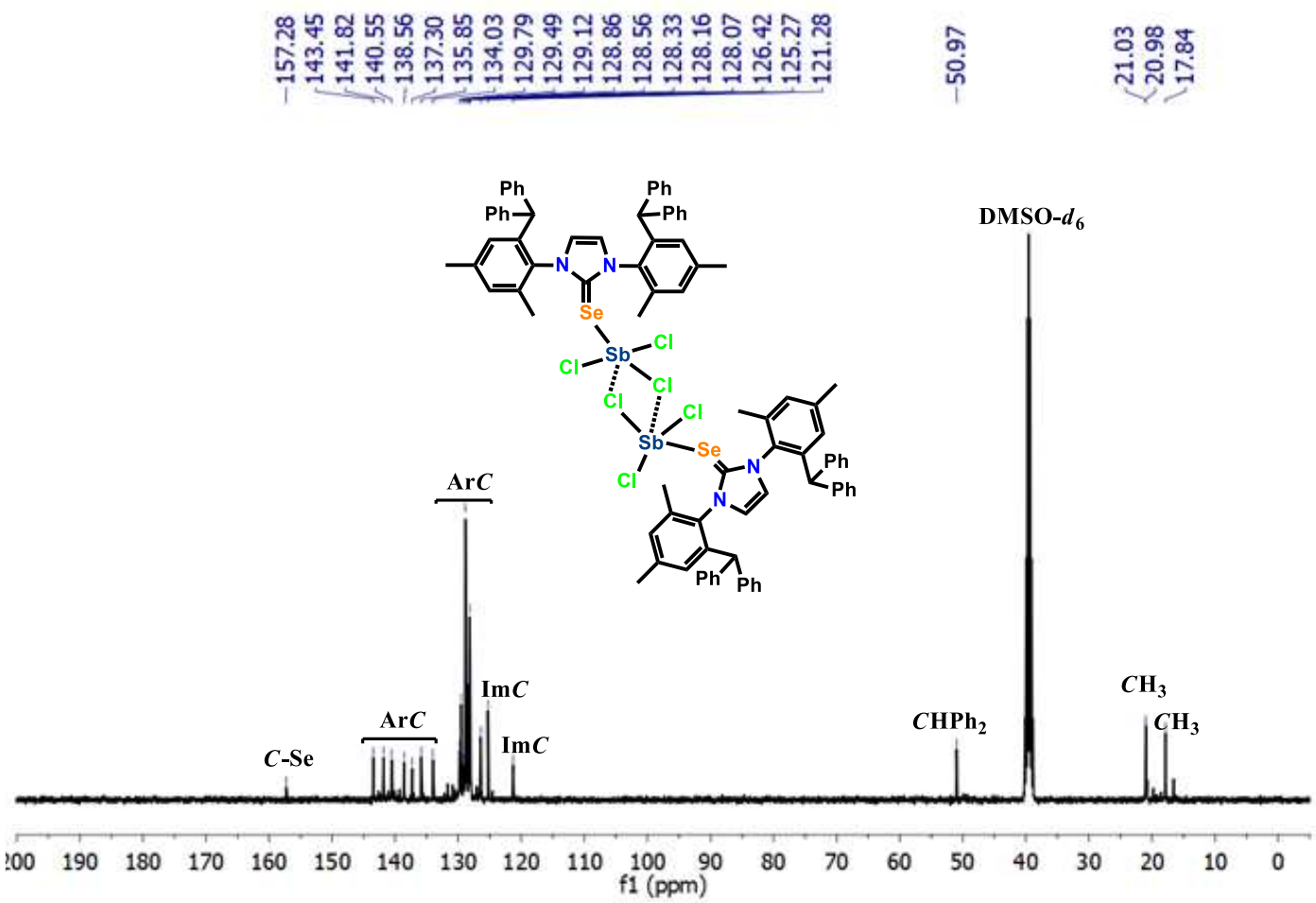

Fig. S7. ^{13}C NMR spectrum of **3** in DMSO- d_6 at 27 °C.

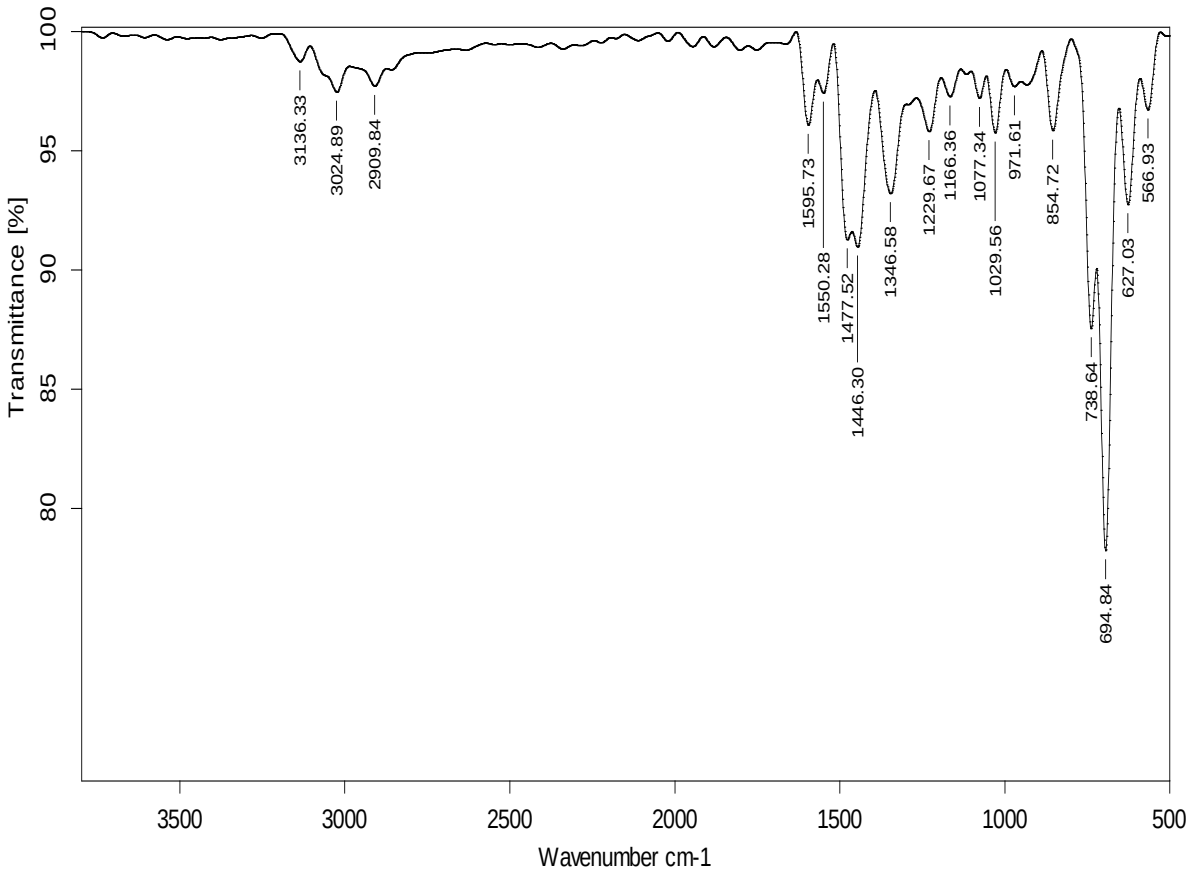

Fig. S8. Neat FT-IR spectrum of **3**.

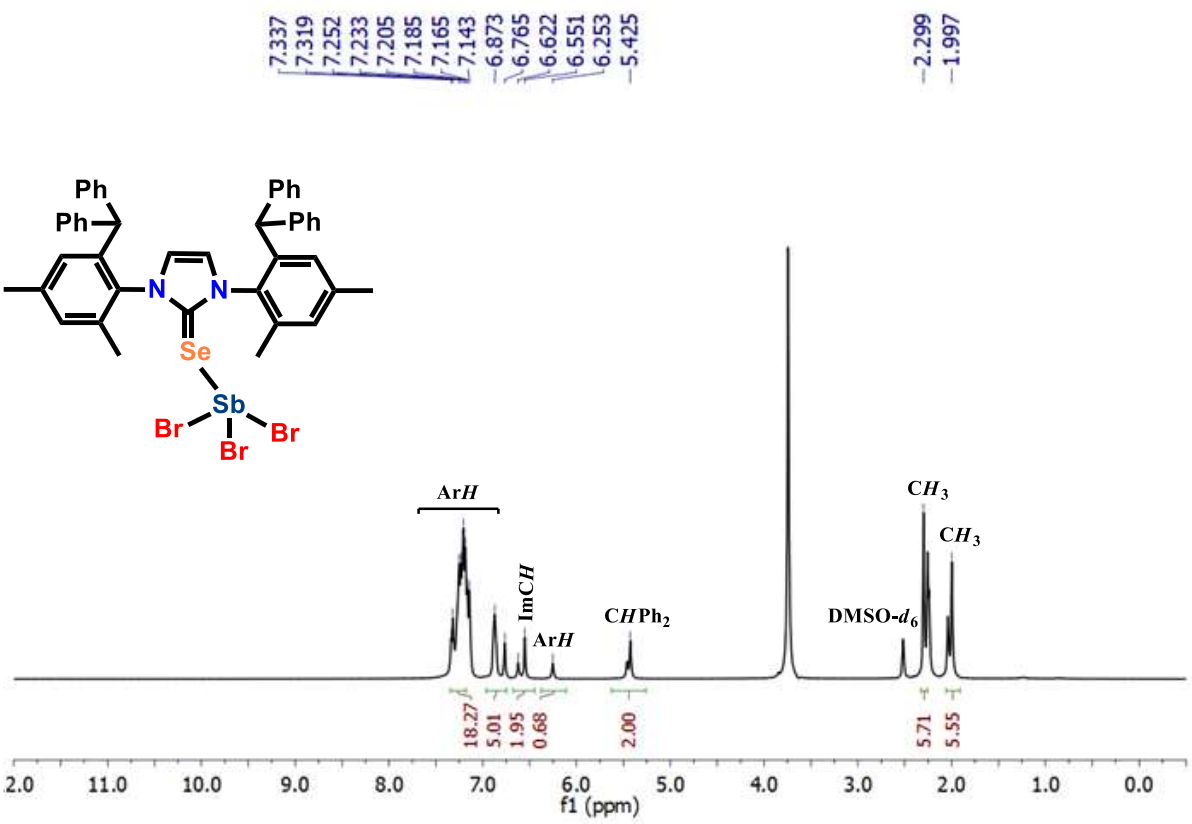

Fig. S9. ^{1}H NMR spectrum of **4** in DMSO-d_6 at 27 °C.

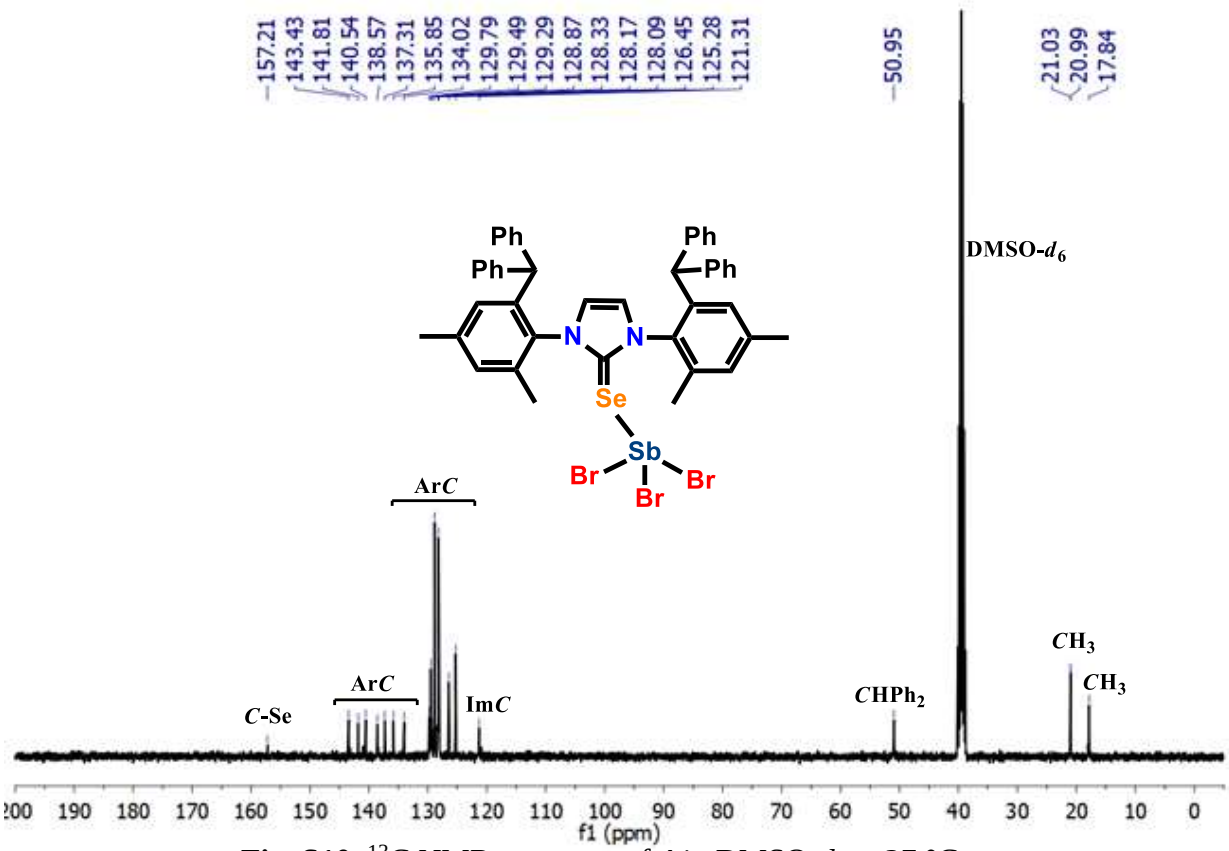

Fig. S10. ^{13}C NMR spectrum of **4** in DMSO-d_6 at 27 °C.

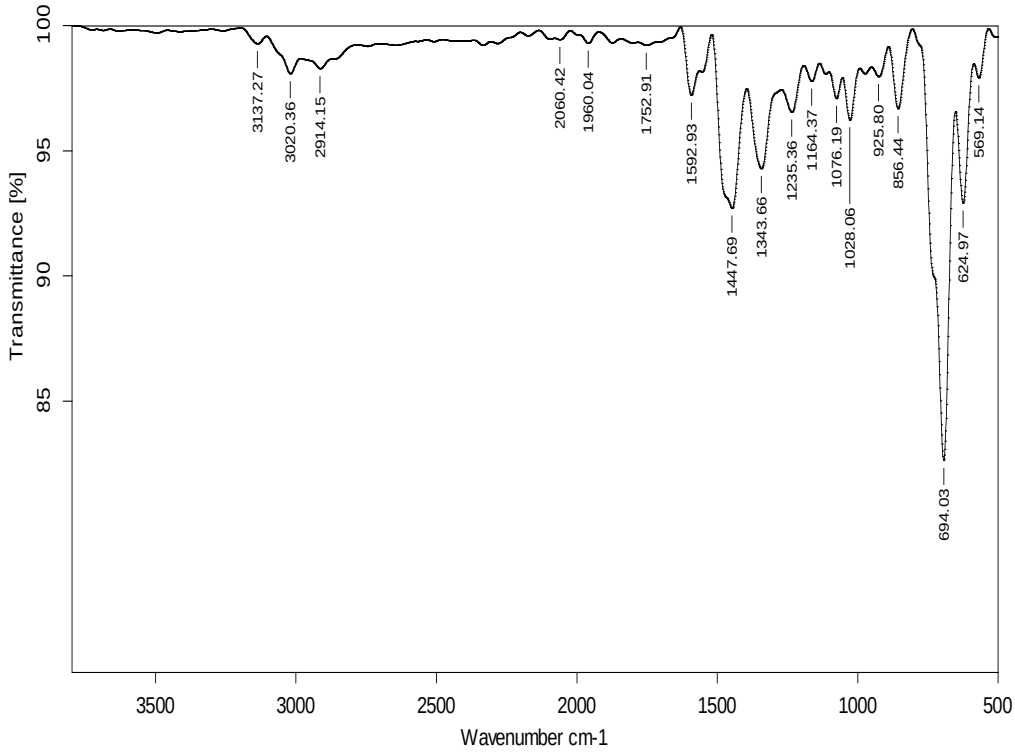

Fig. S11. Neat FT-IR spectrum of **4**.

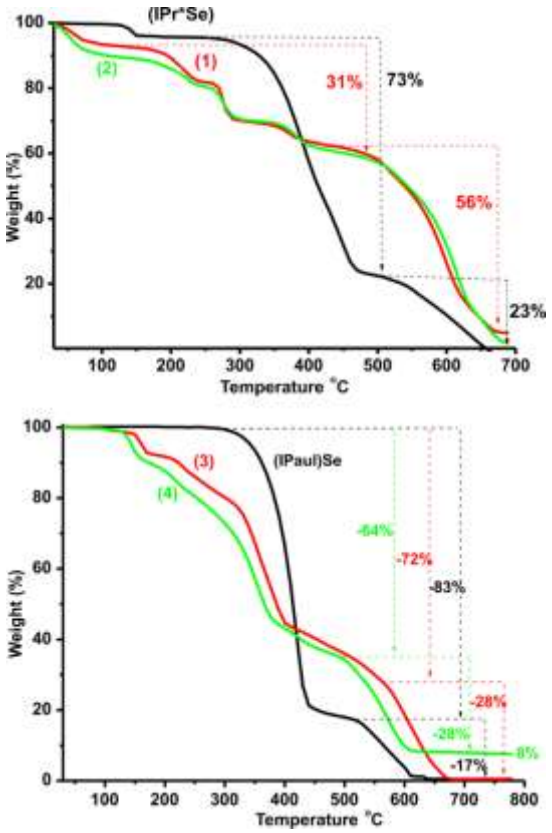

Fig. S12. Top: TGA profiles of IPr*Se, **1**, and **2** from 35 ^{o}C to 700 ^{o}C recorded with a heating rate of 10 ^{o}C min^{-1} under the nitrogen atmosphere. Bottom: TGA curves of [(IPaul)Se], **3**, and **4** from 35 ^{o}C to 800 ^{o}C recorded with a heating rate of 10 ^{o}C min^{-1} under the nitrogen atmosphere.

The thermal stability of **1**, **2**, **3**, and **4** were investigated by thermogravimetric analysis (Fig. S12). The thermal stability of **1**, **2**, **3**, and **4** are compared with the corresponding ligand. The thermal decomposition pathways of the complex are distantly different compared to the ligand. The molecules **1** and **2** decomposed from 35 ^{o}C to 700 ^{o}C. Unlike **1** and **2**, the molecules **3** and **4** decomposed from 110 °C to 670 ^{o}C.

Table S1. Crystal data and structure refinement parameters for **1, 2**, **3,** and **4**.

	1	**2**	**3**	**4**
Empirical formula	$C_{76}H_{62}N_2SeCl_6Sb_2$	$C_{76.33}H_{65.67}N_2Se_1Br_6Sb_2$	$C_{52}H_{48}Cl_3Se_1Sb_1N_2$	$C_{52}H_{48}Se_1Br_3Sb_1N_2$
Formula weight	1538.43	1836.67	1008.05	1141.40
T (K)	298	298	293	293
Crystal system	Monoclinic	Monoclinic	Monoclinic	Monoclinic
Space group	*C1*	*C1*	*P21/c*	*P21/c*
a (Å)	13.6000(3)	13.78581(17)	14.0909(3)	10.17157(19)
b (Å)	23.7029(6)	23.6833(5)	20.4357(4)	23.6916(6)
c (Å)	22.3885(6)	22.4844(4)	17.3498(4)	20.4392(5)
α (°)	90	90	90	90
β (°)	93.718(2)	91.6768(15)	104.844(2)	94.425(2)
γ(°)	90	90	90	90
Volume (Å^3)	7202.0(3)	7337.9(2)	4829.23(17)	4910.78(19)
Z	4	4	4	4
Density (calculated) Mg m^{-3}	1.419	1.663	1.386	1.544
Absorption coefficient mm^{-1}	8.895	10.779	7.188	8.427
F(000)	3080.0	3570.5	2046.7	2250.2
Reflections collected	13692	13542	18971	18443
Independent reflections	8286 [R_{int} = 0.0876, R_{sigma} = 0.0612]	7850 [R_{int} = 0.0314, R_{sigma} = 0.0482]	8956 [R_{int} = 0.0287, R_{sigma} = 0.0384]	9149 [R_{int} = 0.0340, R_{sigma} = 0.0399]
Data/restraints/parameters	8286/626/724	7850/2/724	8956/438/582	9149/0/473
GOF on F^2	1.091	0.952	1.020	1.0298
Final R indexes [I>=2σ (I)]	R_1 = 0.0735, wR_2 = 0.2231	R_1 = 0.0436, wR_2 = 0.1176	R_1 = 0.0321, wR_2 = 0.0873	R_1 = 0.0376, wR_2 = 0.1074
Final R indexes [all data]	R_1 = 0.0777, wR_2 = 0.2278	R_1 = 0.0496, wR_2 = 0.1114	R_1 = 0.0416, wR_2 = 0.0813	R_1 = 0.0478, wR_2 = 0.1074

DFT Calculation[1-3]

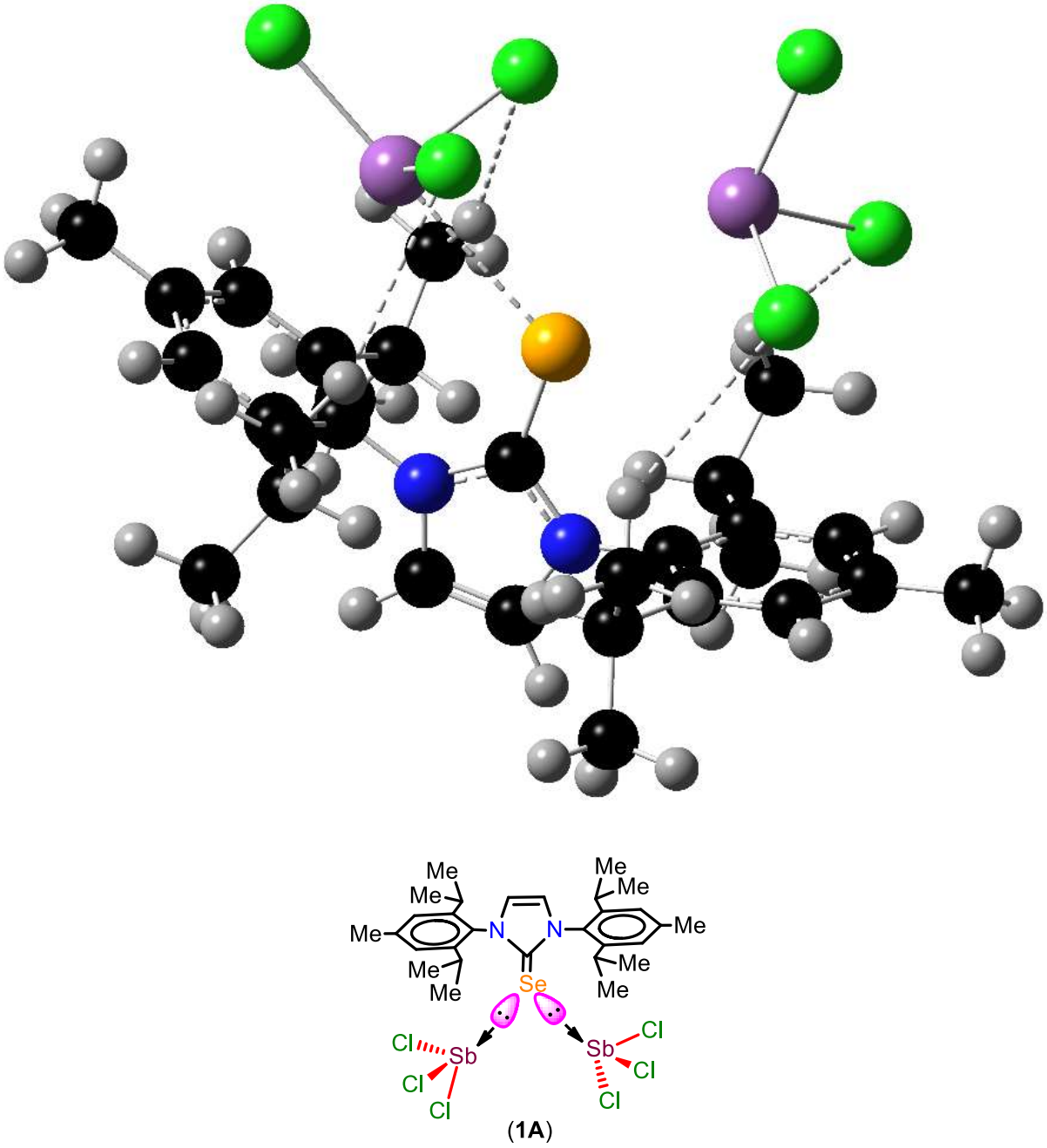

Fig. S13. Optimized geometry of **1A** at the B3LYP/Def2TZVP, 6-31++G** level.

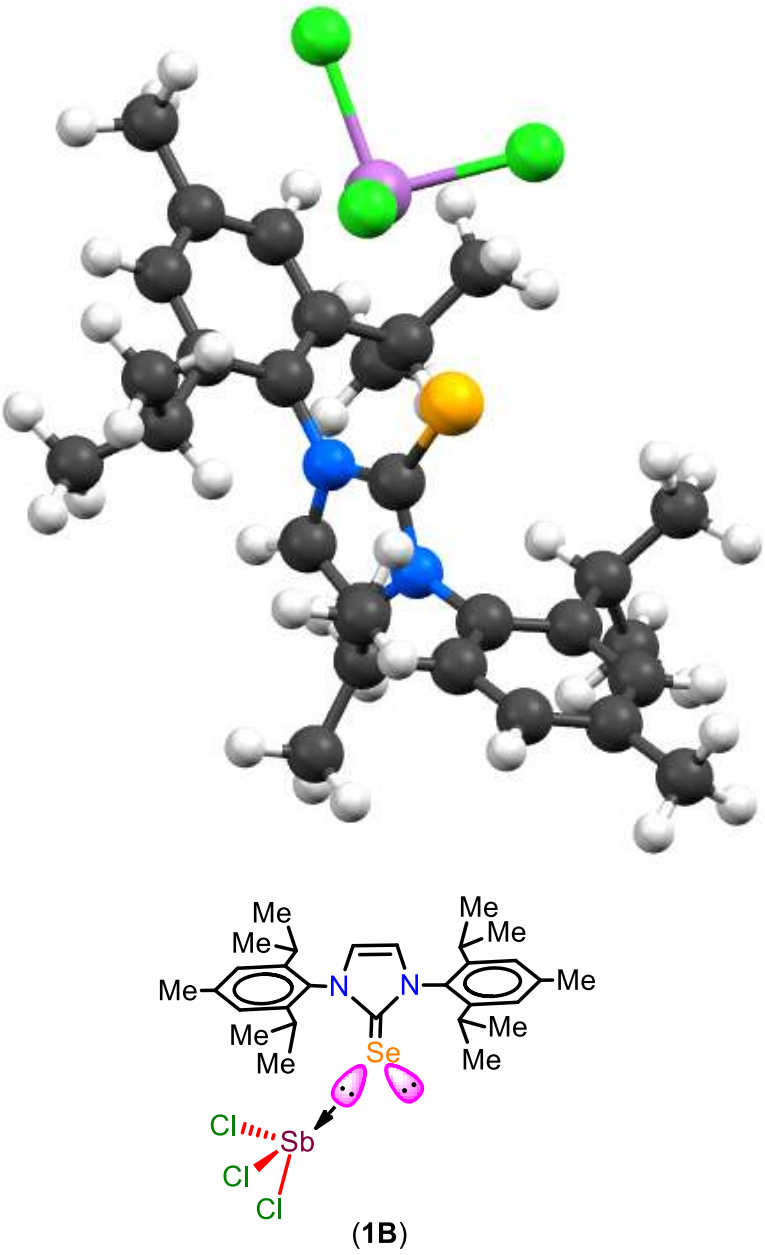

Fig. S14. Optimized geometry of **1B** at the B3LYP/Def2TZVP, 6-31++G** level.

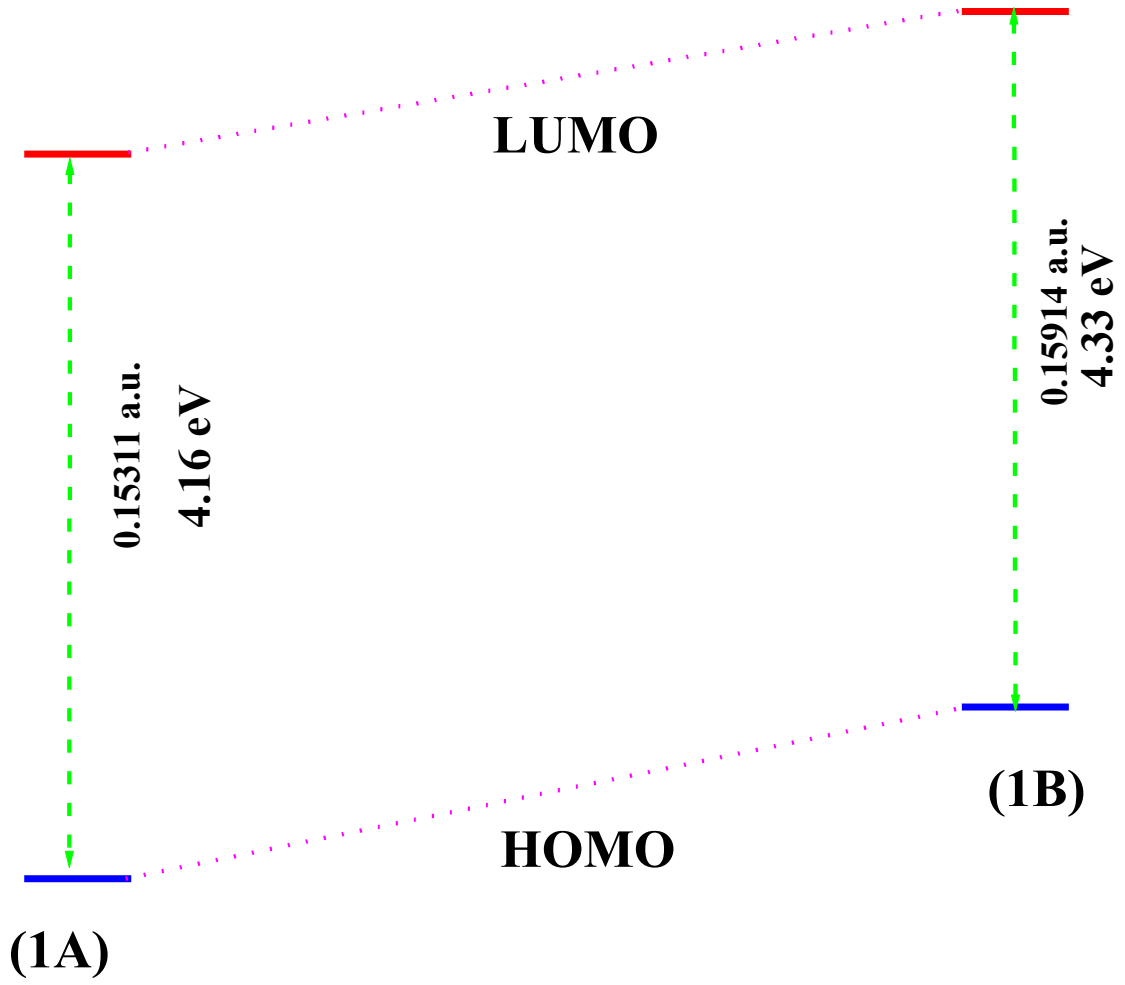

Fig. S15. Comparison of HOMO-LUMO energy gap in **1A** and **1B**.

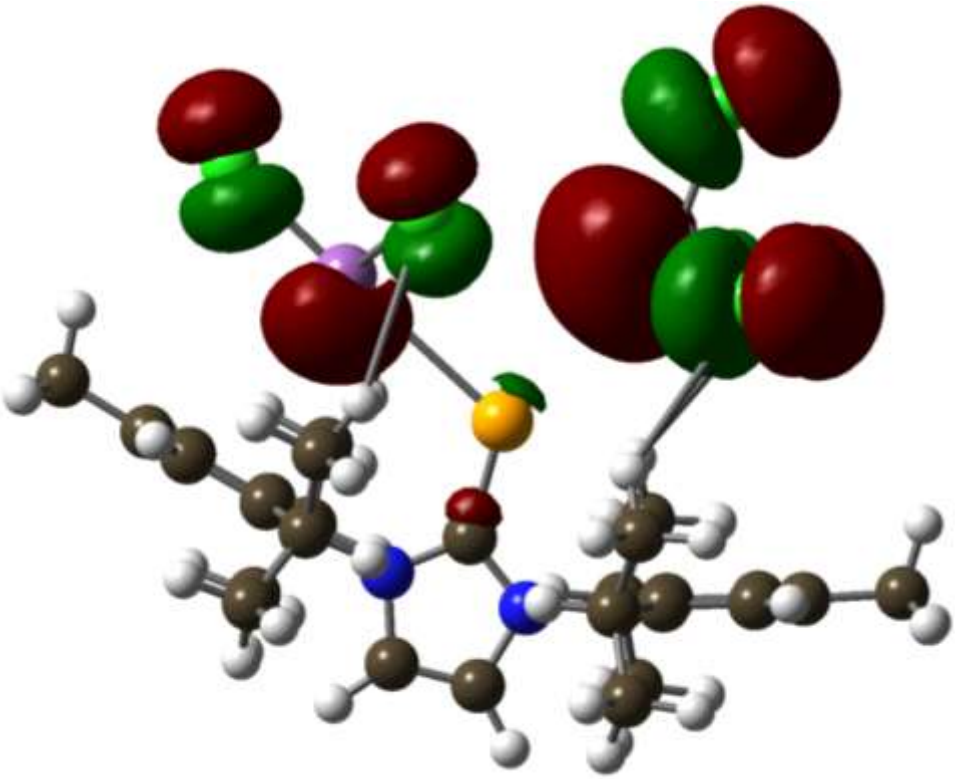

Fig. S16. Lone pairs (HOMO-6) on antimony in **1A.**

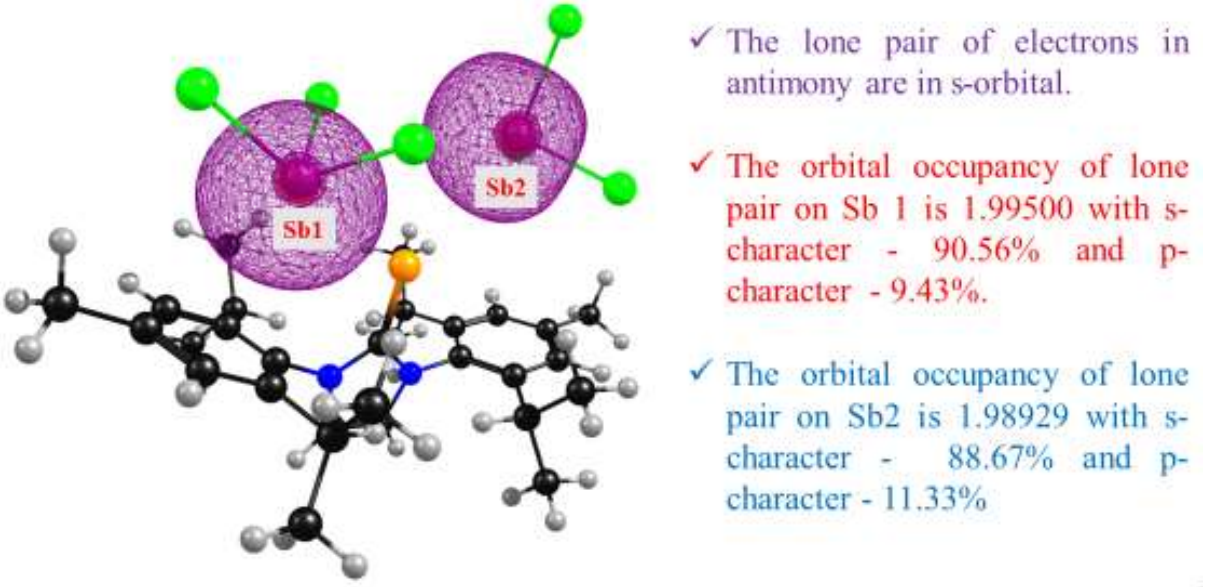

Fig. S17. Lone pair of electrons in **1A.**

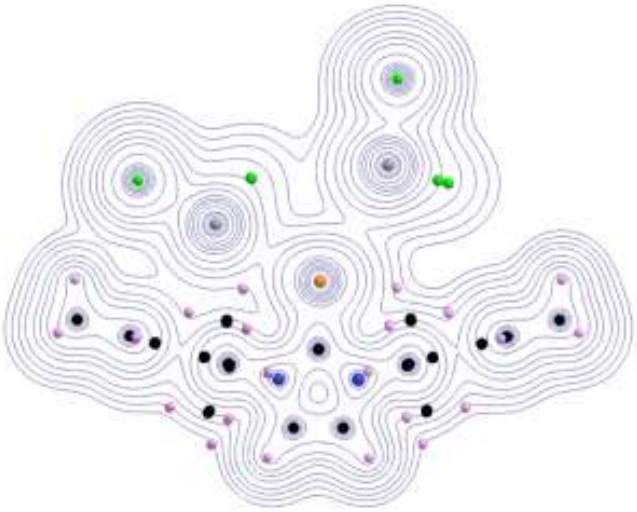

ρ(r) the total charge density is dominated by the electrostatic attraction of the electrons for the positively charged nuclei. The maxima occur at the nuclear sites and ρ(r) decays in a nearly spherical manner away from the nuclei.

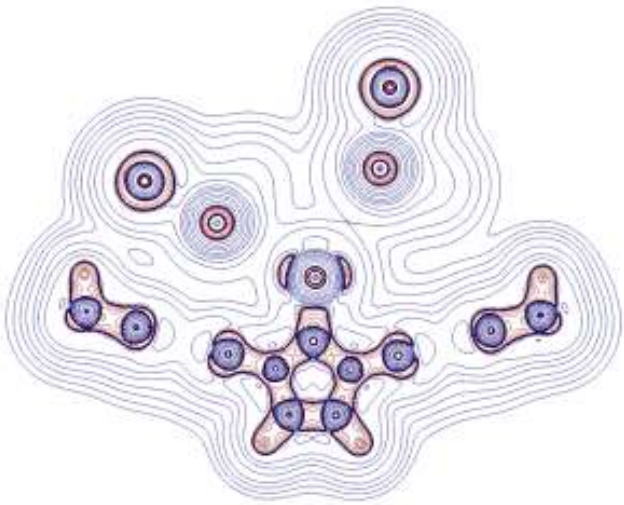

The Laplacian of rho, $\nabla^2(\rho)$, provides a measure of the local charge concentration or depletion. If the value is positive values mean there is local charge depletion (blue) whereas if it is negative values mean there is local charge concentration (red).

Fig S18. AIM analysis of **1A.**

Table S2. The Cartesian coordinates of **1A** optimized at the B3LYP/Def2TZVP,6-31++G** level.

Atom	X	Y	Z
Sb	4.9902037978	18.3617580059	7.3275679391
Cl	5.8569607664	17.4937288942	9.434737155
Cl	5.3223129647	16.332886962	6.0966053414
Cl	7.0401119638	19.3997025235	6.6513659698
Sb	6.7689774021	18.1091356143	2.658761921
Cl	8.8646744845	17.0042824413	2.4344940807
Cl	7.2941378148	19.9894834762	1.2931050245
Cl	5.6105846288	16.8558764058	0.99803329
Se	3.8828707929	19.5062599215	4.4735126589
N	1.6363324182	20.9515911553	3.4087469139
N	1.4444884869	20.6513748434	5.5627071338
C	1.7338268841	19.8676452014	1.2075297046
C	2.2612601336	20.3991899047	4.4929189684
C	2.1236498533	20.9292940629	2.0468705238
C	2.1967071403	19.8902683352	-0.1128411585
H	1.9161858329	19.0826904649	-0.7834044596
C	0.4407048498	21.543113042	3.803753535
H	-0.2030827915	22.0355762399	3.0932626855
C	2.9461861849	21.9834950733	1.6046455663
C	0.3198572746	21.3576276472	5.1409118463
H	-0.4495302394	21.6555073421	5.8344826345
C	3.5418730226	20.8791470114	-2.0141784791
H	2.8498258079	20.360827543	-2.6848880643
H	3.7060570659	21.8881266626	-2.4047801042
H	4.5014560346	20.349387284	-2.0576155739
C	3.3751329716	21.9474394415	0.2732768348
H	4.0142832009	22.7446978466	-0.0960782186
C	3.0188799644	20.9125516389	-0.5973634921
C	2.5718108159	20.7456424723	9.1090203822
H	3.0945817471	21.4133294761	9.7884903185
C	1.6883393007	20.2569024085	6.9295262288
C	2.3764331146	21.1459672844	7.780195561
C	3.3604512631	23.1418889352	2.5077558827
H	3.0216501998	22.9165942887	3.5235661806
C	0.8305835198	18.7314526964	1.6793023222
H	0.6874838387	18.8391078555	2.7588524521
C	2.867575835	22.5152494723	7.3166052582
H	2.7025147053	22.5858209157	6.2376798331
C	0.4118611694	18.0663107575	6.4701235563
H	0.4461288796	18.4659143036	5.4525653275
C	1.4267280708	18.6710115325	8.7144957971
H	1.055576935	17.7197620794	9.0860553722

C	2.1086424265	19.5177361543	9.5965944351
C	1.1991121688	19.0117282258	7.3741850445
C	2.366575921	19.1039444538	11.0259703034
H	2.4160199314	19.9721968055	11.6899495444
H	1.5841069845	18.4341007761	11.3948933936
H	3.3225246579	18.5717552668	11.1053556391
C	-0.5622247206	18.8170065364	1.0201400597
H	-1.2154558887	18.0252674535	1.4039330866
H	-1.0442137276	19.7809549587	1.2172813499
H	-0.4927632411	18.6962762778	-0.0666026613
C	1.4674663235	17.3473654342	1.4478229698
H	1.5853169454	17.1292009679	0.3810641066
H	2.4531733933	17.2810461481	1.9157568013
H	0.8298826766	16.5655384712	1.8755582856
C	-1.0713586997	18.0100904163	6.8943741709
H	-1.5285811321	19.0054858609	6.8974886508
H	-1.6398215197	17.3773224298	6.2040770805
H	-1.1800248294	17.5900944436	7.9004727015
C	1.0235286184	16.6529318015	6.4176249741
H	1.000218492	16.161980894	7.3965185055
H	0.4546899827	16.026019941	5.7225400744
H	2.0607653316	16.6784694259	6.0715967379
C	2.0533157733	23.6452119001	7.9822511293
H	2.1981877421	23.6518962108	9.068228899
H	2.3710624799	24.6199061966	7.5961853203
H	0.9804051634	23.5369417901	7.7898111727
C	4.3777074126	22.7114488562	7.5533031129
H	4.6920301467	23.6875477188	7.1682764653
H	4.6302954534	22.6819177515	8.6187383452
H	4.9658980404	21.9452464298	7.0401038235
C	4.8912470632	23.3084020079	2.5726993032
H	5.3078398915	23.602295346	1.6034056436
H	5.1528541966	24.0897950254	3.2949767278
H	5.3770552001	22.3788487804	2.8808938237
C	2.6780493782	24.4570680768	2.0763347364
H	2.946492092	25.2689276495	2.7616789092
H	2.9909226643	24.7524989713	1.0687446269
H	1.5864843014	24.3631279424	2.0713131781

Table S3. Donor-Acceptor interaction in complex **1A.**

Donor orbital	Acceptor orbital	ΔE kcal/mol	Ei-Ej a.u.	F(I,j) a.u.
n^1_{Se1}	n^{2*}_{Sb1}	4.95	0.58	0.056
n^2_{Se1}	n^{2*}_{Sb1}	48.38	0.09	0.067
n^2_{Se1}	$\sigma^*_{Sb1\text{-}Cl3}$	3.47	0.11	0.018

$n^1_{Se1} \rightarrow n^{2*}_{Sb1}$ $n^2_{Se1} \rightarrow n^{2*}_{Sb1}$ $n^2_{Se1} \rightarrow \sigma^*_{Sb1\text{-}Cl3}$

Table S4. Orbital occupancy, hybridization of orbitals involved in donor-acceptor interaction in **1A.**

Orbital No	Orbital label	Occupancy	Hybridization
182	n^{1}_{Sb1}	1.99500	s(90.56%)p 0.10(9.43%)
183	n^{2*}_{Sb1}	0.58150	s(1.45%)p67.66(98.24%)
194	n^{1}_{Sb2}	1.98929	s(88.67%)p 0.13(11.33%)
204	n^{1}_{Se1}	1.96645	s(82.91%)p 0.21(17.09%)
205	n^{2}_{Se1}	1.77614	s(4.19%)p22.84(95.79%)
206	n^{3}_{Se1}	1.72087	s(0.00%)p 1.00(99.93%)

Orbital No	Orbital label	Occupancy	Coefficients		Hybridization
968	$\sigma^{*}_{Sb1\text{-}Cl3}$	0.10671	77.12%	0.8782*Sb1	s(4.54%)p20.78(94.29%)d 0.19(0.87%)f 0.07(0.30%)
			22.88%	-0.4783*Cl3	s(14.12%)p 6.06(85.63%)d 0.02(0.26%)

Donor orbital	Acceptor orbital	ΔE (E_j-E_i) kcal/mol	E_j-E_i a.u.	F(i,j) a.u.
n^{3}_{Cl4}	$\sigma^{*1}_{Sb1\text{-}Cl3}$	22.45	0.18	0.058
n^{1}_{Cl2}	n^{*2}_{Sb1}	18.20	0.75	0.124
n^{4}_{Cl2}	n^{*2}_{Sb1}	182.08	0.26	0.203
$\sigma^{1}_{C17\text{-}H18}$	$\sigma^{*1}_{Sb1\text{-}Cl3}$	10.31	0.46	0.063

$\sigma^1_{C33-H34}$	$\sigma^{*1}_{Sb1-Cl3}$	20.01	0.36	0.078
$\sigma^1_{C33-C77}$	$\sigma^{*1}_{Sb1-Cl3}$	58.08	0.47	0.151
n^2_{Se9}	n^{*2}_{Sb1}	48.38	0.09	0.067

Table S5. Topological properties of the electron density computed at BCP's for **1A** computed at the B3LYP level.

Bond ellipticity, ε, measures the extent to which density is preferentially accumulated in a given plane containing the bond path. Large ε values indicate structural instability and vice versa. Both Sb1-Se1 and Sb2-Se1 bonds show ε values, which are reasonably small indicating the stable character of binding and probably weak involvement of d-orbitals in bonding.

BCP	Atoms	Rho, ρ(r)	$\nabla^2\rho$	Ellipticity, ε
1	Sb1-Se1	0.021991	+0.033167	0.079727
2	Sb2-Se1	0.008940	+0.020164	0.078488

Table S6. Orbital occupancy – Valence orbitals of **1A**.

Atom	Orbital	Orbital type	Occupancy	Energy
Sb^1	px	Val(5p)	0.55974	-0.15885
Sb^1	py	Val(5p)	0.73188	-0.16708
Sb^1	pz	Val(5p)	0.48602	-0.16133
Sb^2	px	Val(5p)	0.76135	-0.16596
Sb^2	py	Val(5p)	0.51949	-0.15233
Sb^2	pz	Val(5p)	0.49300	-0.15365
Se^1	Px	Val(4p)	1.76173	-0.21723
Se^1	py	Val(4p)	0.91705	-0.16162
Se^1	pz	Val(4p)	1.71914	-0.21851
C^1	px	Val(2p)	0.77674	-0.07889
C^1	py	Val(2p)	1.04666	-0.19098
C^1	pz	Val(2p)	0.96241	-0.18750

Table S7. Natural Population Analysis of **1A**.

Atom	Natural charge	Population			
		Core	Valence	Rydberg	Total
Sb^1	1.28597	45.99788	3.64125	0.07490	49.71403
Sb^2	1.31865	45.99744	3.61126	0.07265	49.68135
Se^1	-0.22536	27.99789	6.20401	0.02346	34.22536
C^1	0.25064	1.99911	3.71132	0.03893	5.74936

Table S8. Electronic configuration of selected atoms of **1A**.

Atom	Electronic configuration
Sb^1	[core]5S(1.86)5p(1.78)6S(0.01)4f(0.01)5d(0.03)6p(0.02)
Sb^2	[core]5S(1.84)5p(1.77)6S(0.01)4f(0.01)5d(0.03)6p(0.01)
Se^1	[core]4S(1.81)4p(4.40)4d(0.01)6S(0.01)6p(0.01)
C^1	[core]2S(0.93)2p(2.79)3d(0.01)4p(0.02)

Table S9. Wiberg Bond Index of **1A**.

Bond	Bond order
Sb^1-Se^1	0.2146
Sb^2-Se^1	0.0478
Se^1-C^1	1.2505

Table S10. The Cartesian coordinates of **1C** optimized at the B3LYP/Def2TZVP, 6-31++G** level.

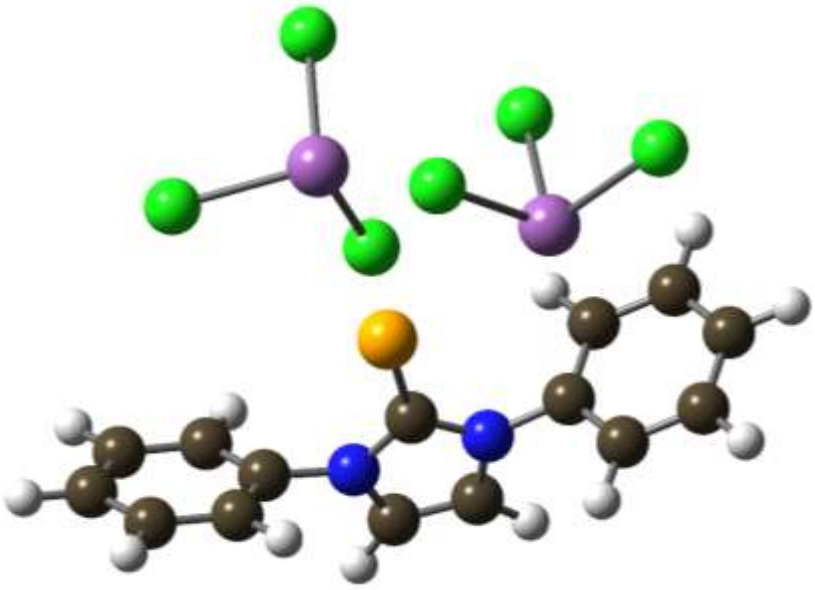

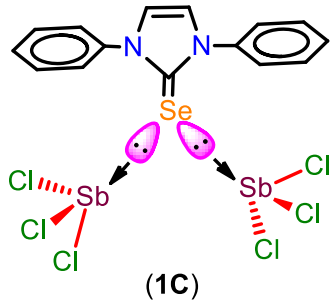

(**1C**)

Atom	X	Y	Z
Sb	-2.4779234683	1.7757086152	-1.4208758921
Cl	-4.3368285367	3.213091577	-2.0066453292
Cl	-1.9915167879	2.894791577	0.6537746218
Cl	-0.8619434129	2.9294760523	-2.7348731362
Sb	1.3791423301	1.8446966073	1.4562018116
Cl	1.5894990018	3.3977575876	3.2769397567
Cl	3.6967764875	1.2761361897	1.3233959662
Cl	0.7254517031	-0.0107955828	2.8480961432
Se	0.1973162078	-0.1703438134	-1.1181748263
N	0.9367592819	-2.7164185092	0.0093220654

N	-1.1798298434	-2.3102393517	0.3081756715
C	3.2958459247	-2.4239850012	0.5779084797
C	-0.03693387	-1.7870638358	-0.2297050026
C	2.3182005966	-2.6353446612	-0.3944842763
C	4.6391583423	-2.3989921401	0.1947767761
H	5.4054623008	-2.222115789	0.9427012881
C	0.4046147014	-3.8001289159	0.7003791945
H	1.0169350126	-4.6402087853	0.9850773258
C	2.6541942826	-2.8190251833	-1.7377170243
C	-0.9135717539	-3.5492939596	0.885929749
H	-1.6869015987	-4.1202038133	1.3735290051
C	3.9986799445	-2.7865652795	-2.1100504945
H	4.2702248692	-2.9212952006	-3.1525247945
C	4.9903255553	-2.5799075152	-1.145180338
C	-4.6915331308	-1.5840751522	-0.6884764488
H	-5.4004434213	-1.8799512322	-1.4556331124
C	-2.4917685129	-1.7180673579	0.288991463
C	-3.3963532702	-2.1081650495	-0.7024051146
C	-4.1547335713	-0.2961293551	1.2943078121
H	-4.4443638205	0.411833207	2.0642360913
C	-5.0711565949	-0.6801653597	0.3096277735
C	-2.857197899	-0.8177152812	1.291725538
H	-3.085206152	-2.808174175	-1.4716152683
H	-2.1326572554	-0.5256249483	2.0447633801
H	1.8734887638	-2.9718974495	-2.4753627992
H	3.0064822735	-2.2562553833	1.6101687297
H	-6.0764108308	-0.2702536888	0.3160864793
H	6.0350985115	-2.5528270631	-1.4398035347

Table S11. The Cartesian coordinates of **1D** optimized at the B3LYP/Def2TZVP, 6-31++G** level.

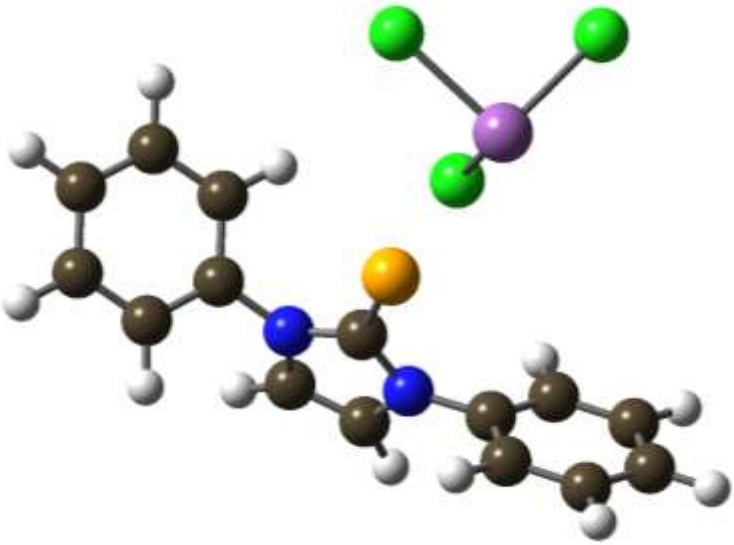

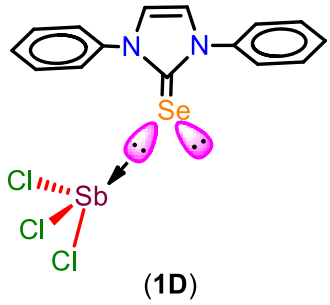

(**1D**)

Atom	X	Y	Z
Sb	-1.3682376787	-2.2459879284	-0.9976776225
Cl	-2.7833884162	-3.2724607002	-2.7039111698
Cl	-0.3762646781	-0.6869670951	-2.5390624104
Cl	0.3511321081	-3.8995506677	-1.1052824475
Se	0.2001811642	-0.6741961668	1.3443883526
N	2.1083933211	0.9793581869	-0.0643319923
N	0.1491564347	1.9220537842	0.062742074
C	3.212432354	-1.1431840404	-0.6168492398
C	0.8384870022	0.7899145989	0.4114483284
C	3.2172310357	0.0714216271	0.0708994574

C	4.3159246784	-1.9902884336	-0.4998452749
H	4.3150528563	-2.940179976	-1.0251083284
C	2.2016352565	2.2104252488	-0.7049719535
H	3.1207496429	2.5389944744	-1.1619847047
C	4.3036049768	0.4540033811	0.8610248877
C	0.981883864	2.7962073763	-0.6285944236
H	0.6251912812	3.746048188	-0.9921370998
C	5.406003557	-0.3978361762	0.964610024
H	6.2527488788	-0.1089872352	1.5798959322
C	5.4118750847	-1.6195058969	0.2855027346
C	-2.9945801526	2.7107678887	1.8994187801
H	-3.3297009393	2.8680246172	2.9200941382
C	-1.2348184246	2.1982256865	0.3383226452
C	-1.655226154	2.4038801726	1.6542700353
C	-3.4667627578	2.6085139766	-0.4742149869
H	-4.167681688	2.6811086181	-1.3002001049
C	-3.9000727332	2.8148758665	0.8382346247
C	-2.1286441005	2.2962496705	-0.730295122
H	6.2672130082	-2.2831805516	0.3709673382
H	4.2773420762	1.3983291538	1.396419501
H	2.3584626856	-1.4212417489	-1.2233032278
H	-0.9451203985	2.3118026757	2.468535652
H	-1.7826756698	2.1087153072	-1.7416486711
H	-4.9411147753	3.0531895877	1.0349555243

Crystallographic analysis of 1-4

Structure 1:

Structure **1** gave one "B" level alert as PLAT342_ALERT_3_B Low Bond Precision on C-C Bonds 0.02545 Ang., due to the largest Z (max) >39. The solvent molecule in **1** with the unit cell volume of 547.8 A^3 and electron counts of 95.3 could not be modelled satisfactorily. Therefore, the electron densities arising from a disordered toluene molecule were removed from the electron density map by the SQUEEZE treatment using the OLEX2 solvent mask command. The SQUEEZE result reflected the elimination of 95.3 electrons from the unit cell. One toluene molecule (a total number of electrons = 50 electrons) and one CH_2Cl_2 (a total number of electrons for CH_2Cl_2 = 42 electrons) were accounted for per unit cell. The early decomposition of **1** in TGA also supports this assessment (*vide supra*). The weight loss (10%) from 35 ^oC to 110 ^oC in TGA can be attributed to the lattice solvent molecules (Calculated 10%). Data reduction, scaling, and absorption corrections were performed using CrysAlisPro (Rigaku, V1.171.38.46, 2015). The final completeness is 99.90 % out to 69.987° in θ. Refined as a 2-component twin. The completeness statistics refer to single and composite reflections containing twin-component ones only.

Structure 2:

No "A" level and "B" level alerts. The solvent molecule in **2** with 65 electrons per asymmetric unit could not be modelled satisfactorily. Therefore, the electron densities arising from disordered solvent molecules were removed from the electron density map by the SQUEEZE treatment using the OLEX2 solvent mask command. The SQUEEZE result reflected the elimination of 65 electrons per asymmetric unit. One toluene (a total number of electrons for one toluene = 50 electrons) and 1/3 CH_2Cl_2 (a total number of electrons for

1/3 CH_2Cl_2 = 15 electrons) were accounted per asymmetric unit. The early decomposition of **2** in TGA also supports this assessment (*vide supra*). The weight loss (8%) from 35 ^oC to 110 ^oC in TGA can be attributed close to a calculated weight loss of one toluene and 1/3 CH_2Cl_2 (Calculated 6%).

Structure 3:

The following two "A" level alerts were observed due to solvent-accessible void in the structure. PLAT043_ALERT_1_A Calculated and Reported Mol. Weight Differ by 184.38. PLAT602_ALERT_2_A Solvent Accessible VOID(S) in Structure. The solvent molecule in **3** with the unit cell volume of 484.1 A^3 and an electron count of 103.8 could not be modelled satisfactorily. Therefore, the electron densities arising from a disordered toluene molecules were removed from the electron density map by the SQUEEZE treatment using the OLEX2 solvent mask command. The SQUEEZE result reflected the elimination of 103.8 electrons from the unit cell. Two toluene molecules (a total number of electrons = 50 electrons) were accounted for per unit cell. However, the weight loss for the toluene molecule was not detected in TGA, which could be due to the loss of the solvent molecule during the sample preparation.

Structure 4:

No "A" level and "B" level alerts. The solvent molecule in **4** with the unit cell volume of 269.4 A^3 and electron counts of 56.4 could not be modelled satisfactorily. Therefore, the electron densities arising from a disordered toluene molecule were removed from the electron density map by the SQUEEZE treatment using the OLEX2 solvent mask command. The SQUEEZE result reflected the elimination of 56 electrons from the unit cell. One toluene (a total number of electrons for one toluene = 50 electrons) was accounted for per unit cell. However, the weight

loss for the toluene molecule was not detected in TGA, which could be due to the loss of the solvent molecule during the sample preparation.

References

(1) Gaussian 16, Revision A.03, M. J. Frisch, G. W. Trucks, H. B. Schlegel, G. E. Scuseria, M. A. Robb, J. R. Cheeseman, G. Scalmani, V. Barone, G. A. Petersson, H. Nakatsuji, X. Li, M. Caricato, A. V. Marenich, J. Bloino, B. G. Janesko, R. Gomperts, B. Mennucci, H. P. Hratchian, J. V. Ortiz, A. F. Izmaylov, J. L. Sonnenberg, D. Williams-Young, F. Ding, F. Lipparini, F. Egidi, J. Goings, B. Peng, A. Petrone, T. Henderson, D. Ranasinghe, V. G. Zakrzewski, J. Gao, N. Rega, G. Zheng, W. Liang, M. Hada, M. Ehara, K. Toyota, R. Fukuda, J. Hasegawa, M. Ishida, T. Nakajima, Y. Honda, O. Kitao, H. Nakai, T. Vreven, K. Throssell, J. A. Montgomery, Jr., J. E. Peralta, F. Ogliaro, M. J. Bearpark, J. J. Heyd, E. N. Brothers, K. N. Kudin, V. N. Staroverov, T. A. Keith, R. Kobayashi, J. Normand, K. Raghavachari, A. P. Rendell, J. C. Burant, S. S. Iyengar, J. Tomasi, M. Cossi, J. M. Millam, M. Klene, C. Adamo, R. Cammi, J. W. Ochterski, R. L. Martin, K. Morokuma, O. Farkas, J. B. Foresman, and D. J. Fox, Gaussian, Inc., Wallingford CT, 2016.

(2) GaussView, Version 6, Dennington, R.; Keith, T. A.; Millam, J. M. Semichem Inc., Shawnee Mission, KS, 2016.

(3) (a) AIMAll (Version 19.10.12), Keith, T. A.; TK Gristmill Software, Overland Park KS, USA, 2019; (b) Bader, R. F. W. *Atoms in Molecules: A Quantum Theory*; Oxford University Press: New York, 1990.